Optical Patterning of Photosensitive Thin Film Silica Mesophases

Dhaval A. Doshi*, Nicola K. Huesing†, Mengcheng Lu*, Hongyou Fan*, Alan J. Hurd‡, C. Jeffrey Brinker*‡

*University of New Mexico/NSF Center for Micro-Engineered Materials, Advanced Materials Laboratory, 1001 University Boulevard SE, Albuquerque, New Mexico 87106, USA

† Institute of Inorganic Chemistry, Vienna University of Technology, Vienna, Austria

‡ Sandia National Laboratories, Catalytic and Porous Materials Department, 1841, Albuquerque, New Mexico, 87185, USA

Photosensitive films incorporating molecular photoacid generators compartmentalized within a silica-surfactant mesophase were prepared by an evaporation-induced self-assembly process. UV-exposure promoted localized acid-catalyzed siloxane condensation, enabling selective etching of unexposed regions, thereby serving as a 'resistless' technique to prepare patterned mesoporous silica. We also demonstrated an optically-defined mesophase transformation (hexagonal→tetragonal) and patterning of refractive index and wetting behavior. Spatial control of structure and function on the macro- and mesoscales is of interest for sensor arrays, nano-reactors, photonic and fluidic devices, and low dielectric constant films. More importantly, it extends the capabilities of conventional lithography from spatially defining the presence or absence of film to spatial control of film structure and function.

Since the discovery of surfactant-templating procedures to prepare ordered mesoporous silicas (1), films have been identified as a promising application. Thin film silica mesophases have been prepared at solid-liquid (2) and liquid-vapor interfaces (3), and by spin-coating (4, 5), and dip-coating (6, 7). These procedures have been combined with soft lithographic techniques

DISCLAIMER

(8) to create patterned films (9, 10). However such techniques required long processing times and have been limited to physically defining the presence or absence of film (9, 10). For sensor arrays and micro-fluidic devices, it is of interest to pattern the thin film mesostructure (for example, hexagonal versus cubic or disordered), thereby spatially controlling properties like refractive index and accessibility of the mesoporosity to a fluid phase.

Our process exploits the pH-sensitivity of both the siloxane condensation rate and the silica-surfactant self-assembly process to chemically define film presence or absence as well as to spatially control mesostructure and properties. We begin with a homogeneous solution of silica, surfactant, photoacid generator (PAG, a diaryliodonium salt) and HCl (11) with initial acid concentration designed to minimize the siloxane condensation rate (12, 13). Preferential ethanol evaporation during dip- or spin-coating (14) concentrates the depositing solution in water and non-volatile constituents, thereby promoting self-assembly (6, 15) into a photosensitive, one-dimensional (1-dH) silica/surfactant mesophase. Due to chemical modification with a long-chain hydrocarbon, the PAG serves as a co-surfactant during the assembly process, promoting its uniform incorporation within the mesostructured channels of the 1-dH film.

Irradiation of the PAG at λ_{max} = 256 nm results in homolytic or heterolytic photodecomposition to yield the Brønsted super-acid, $H^+SbF_6^-$, plus an iodoaromatic compound and organic by-products (16):

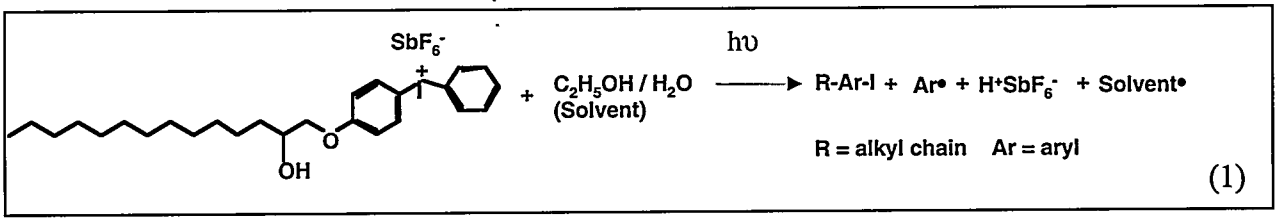

(1)

UV exposure of the photosensitive mesophase through a mask creates patterned regions of differing acid concentrations (Fig. 1). Co-incorporation of a pH-sensitive dye (ethyl violet)

allows direct imaging of these patterned regions as shown in Fig. 2a, where the yellow (exposed) and blue (masked) regions correspond to pH 0 and pH 2, respectively (17).

Suppression of the siloxane condensation rate during film deposition enables several modes of optically-mediated patterning. First, since acid generation promotes siloxane condensation, selective UV exposure results in patterned regions of more and less highly condensed silica (18). Differential extents of siloxane condensation result in turn in differential solubility, allowing selective etching of more weakly condensed regions in aqueous base (0.2 M NaOH). Figure 2b shows an optical micrograph of a UV-exposed and etched thin film mesophase after calcination to remove the surfactant templates. Consistent with Figure 1, we observe a lithographically-defined pattern of mesoporous mesas, *i.e.* film is present in the exposed regions and absent in the un-exposed regions. The plan-view TEM micrograph (Fig. 2b inset) reveals a striped mesoscopic structure consistent with a 1-dH mesophase with unit cell size $a = 37$ Å. This process eliminates the need for a photoresist in the patterning of mesoporous low κ films needed by the microelectronics industry (19).

Second, when we calcine (rather than etch) the optically-patterned films, we effect the patterning of film thickness and refractive index as evinced by the optical interference image shown in Fig 2c. Spectroscopic ellipsometry indicates that the UV-exposed regions are thicker with greater pore volume and lower refractive index (see Table 1). As discussed below these differences largely stem from a hexagonal to tetragonal mesophase transformation. Significantly the refractive index contrast (Δn = 0.025 at 630nm) (20) is sufficient to make optical waveguides (21).

A third aspect of this approach is photo-definable wetting behavior. Photolysis of PAG produces organic by-products (Eqn. 1) that render UV-exposed regions more hydrophobic

(contact angle = 40°) than unexposed regions (contact angle <10°). Figure 2d shows that patterned hydrophobic regions serve as corrals for water. Such corrals (22) are of great interest for creating sensor arrays, e.g. by selective derivatization of the hydrophilic areas with aqueous-based precursors or bio-molecules.

A final aspect of our approach is the optically-defined transformation of the mesophase structure (nanostructural lithography). Figure 3 compares thin film X-ray diffraction (XRD) patterns of unirradiated and irradiated samples after calcination at 450°C to remove surfactant. Also shown is the XRD pattern of an unirradiated PAG-containing film exposed to HCl vapor (14) prior to calcination. The XRD pattern of the unirradiated film (Figure 3, trace A) is consistent with a 1-dH mesophase with lattice constant a = 42.1 Å, whereas the pattern of the irradiated sample (Figure 3 trace B) is assigned to a mixture of a tetragonal (distorted cubic) mesophase with a = 66.8 Å and $b = c$ = 72.8 Å (23) and the un-transformed parent structure, a 1-dH mesophase with a = 38.5 Å (24). The XRD pattern of the HCl-exposed sample is comparable to that of the irradiated sample but shifted to higher d-spacing. TEM images of the corresponding unirradiated and irradiated calcined films are shown in Figure 4. The cross-sectional TEM image of the unirradiated film (Figure 4A) reveals a striped pattern characteristic of the [110]-orientation of a 1-dH mesophase (a = 42.7 Å), with mesopore channels oriented parallel to the substrate surface. The cross-sectional TEM image of the irradiated film exhibits predominantly a diamond-shaped texture consistent with the [010]-orientation of a tetragonal mesophase, however the occasional presence of horizontal stripes suggests an incomplete 1-dH → tetragonal phase transformation. The magnified image of the striped and diamond textures (Figure 4 A and 4B insets) points out the topotactic relationship between the 1-dH and tetragonal

mesophases and suggests that the transformation results in a factor of $\sqrt{3}$ increase in lattice constant consistent with the mechanism proposed below.

For the supported thin film mesophases adhesion to the substrate can distort the mesostructure and influence the phase transformation process. To avoid this complication and enable acquisition of powder XRD patterns, we detached the films before irradiation and calcination. Figure 5 compares powder XRD patterns of the unirradiated and irradiated specimens after calcination. Similar to results for comparable, attached films, the XRD pattern of the unirradiated powder is consistent with 1-dH (a = 52.8Å), while that of the irradiated powder is consistent with tetragonal ($a = b$ = 81.5 Å and c = 107.8 Å) (23, 24). The smaller lattice dimension observed for attached film (Figure 3) compared to powder (Figure 5) results from polymerization-induced shrinkage occurring in the unconstrained direction (normal to the substrate) probed by X-ray reflectivity experiments. Corresponding TEM images of the calcined powders (Fig. 6) show hexagonal and tetragonal mesostructures consistent with the XRD results.

Having chosen the initial acid concentration to minimize the siloxane condensation rate (12, 13) we argue that the as-deposited film represents the thermodynamically favored surfactant-oligomeric silica mesophase; the evaporation-induced self-assembly process is not kinetically inhibited by any significant amount of silica condensation accompanying film deposition. As shown in Figure 2a, the effective pH of the as-deposited mesophase (pH~2) is much less than the pKa of the silicate oligomers, pKa = 6.5 (25), causing the framework to be protonated. At pH 2, the protonated framework (I) interacts with the protonated ethylene oxide (EO) blocks of the surfactant head groups via an $R\text{-}EO_{m-y}[(EO)_y\bullet(H_3O^+)_z]\bullet\bullet\bullet zX^-\bullet\bullet\bullet wI^{\delta+}$ mechanism (where m = number of EO blocks in the surfactant, y = number of hydrogen-bonded EO blocks making up the hydrophilic headgroup, z = number of hydronium ions attached to the

EO blocks, X, the anionic species, w= number of silica tetrahedra co-assembling, and δ, the network charge) in which the positive charge of the framework and surfactant is mediated by the charge of the Cl^- and SbF_6^- anions. Photo-generation of acid promotes siloxane condensation as shown by ^{29}Si NMR results along with decreased film thickness, a reduction in XRD d-spacing, and development of appreciable biaxial tension as measured using a cantilever beam (26). Subsequent heating promotes further siloxane condensation (26) and at 125°C we observe by XRD and TEM the 1dH→ tetragonal phase transformation.

The mechanism of the phase transformation may be understood by consideration of how silica/surfactant mesophases reorganize in response to increased extents of siloxane condensation. It is generally believed that the factors governing the formation of a specific silica-surfactant mesophase are the same as those governing corresponding surfactant-water mesophases. The thermodynamically favored phase is that which allows the surfactant headgroup area a to be closest to its optimal value a_o, while maintaining favorable packing of the hydrophobic surfactant tails (27, 28). The influence of a_o along with the surfactant volume v and tail length l on the resultant mesophase can be understood qualitatively by the dimensionless packing parameter $g = v/a_o l$: where $g = 1$ favors formation of vesicles, bilayers, or lamellar mesophases and decreasing values of g result in the formation of progressively higher curvature mesophases and ultimately spherical micelles ($g < 1/3$) (27, 28). Monnier et al. (29) introduced the term G_{inter} in their free energy expression to account for electrostatic interactions between the silica framework and surfactant head groups. When the framework charge density matches the average surface charge density of the surfactant head groups $1/a$, G_{inter} is minimized, establishing a_o, which in turn influences g and the mesophase curvature.

In the present study, condensation of the silica framework substantially increases its acidity as reflected by a reduced pKa and isoelectric point (12). Therefore, although the overall pH of the system is reduced by photo-induced acid generation, the protonation of the silica framework decreases relative to that of the ethylene oxide headgroups. In order to maintain charge density matching at the silica-surfactant interface, the optimal ethylene oxide headgroup area a_o must increase. The increased value of a_o in turn reduces the surfactant packing parameter g, favoring transformation to a higher curvature mesophase.

Mechanistically, we propose the phase transformation proceeds through creation of periodic undulations along the length of the closed packed cylindrical channels of the 1-dH mesophase, as is known for the temperature-induced hexagonal to body-centered-cubic transformation of $C_{12}EO_{12}$ in the $C_{12}EO_{12}/H_2O$ binary system (30). For the silica-surfactant system undulation results finally in a tetragonal (distorted cubic) packing as depicted in Figure 7. d_{100} for the parent 1-dH mesophase becomes d_{200} of the tetragonal mesophase, resulting in a factor of $\sqrt{3}$ increase in the lattice parameter. Distortion arises due to condensation occurring preferentially normal to the substrate. The 1-dH $\rightarrow$ tetragonal phase transformation occurs with minimal displacement of the silica oligomers and surfactant species, and we expect a precise topotactic relationship between the hexagonal and tetragonal mesophases as shown schematically in Fig.7 and by TEM in Figs. 4A and 4B. There are two previous reports of condensation-driven transformations to higher curvature mesophases, lamellar $\rightarrow$ 1-dH (29) and lamellar $\rightarrow$ cubic (6), but our study appears to be the first report of a hexagonal to cubic or tetragonal transformation. Since it depends critically on the initial surfactant and acid concentrations (31), the transformation may be realized or avoided by judicious choice of these parameters.

We anticipate that the procedures reported here will extend the capabilities of conventional lithography from patterning the presence or absence of films to the spatial definition of both thin film structure and properties. As such this optical patterning technique should find application as an alternative to micro-machining in the construction of microsystems and, ultimately, nanosystems, where it would be desirable to define and integrate multiple functions (e.g. fluidic and photonic) with high areal densities.

1. C. T. Kresge, M. E. Leonowicz, W. J. Roth, J. C. Vartuli, J. S. Beck, *Nature* **359**, 710-712 (1992).

2. H. Yang, A. Kuperman, N. Coombs, S. Mamicheafara, G. A. Ozin, *Nature* **379**, 703-705 (1996).

3. H. Yang, N. Coombs, I. Sokolov, G. A. Ozin, *Nature* **381**, 589-592 (1996).

4. M. Ogawa, *Journal of the American Chemical Society* **116**, 7941-7942 (1994).

5. M. Ogawa, *Chemical Communications* , 1149-1150 (1996).

6. Y. F. Lu, et al., *Nature* **389**, 364-368 (1997).

7. D. Zhao, et al., *Advanced Materials* **10**, 1380-1385 (1998).

8. Y. N. Xia, G. M. Whitesides, *Annual Review of Materials Science* **28**, 153-184 (1998).

9. M. Trau, et al., *Nature* **390**, 674-676 (1997).

10. P. D. Yang, et al., *Science* **282**, 2244-2246 (1998).

11. Precursor solutions were prepared by addition of the surfactant and the PAG (a diaryliodonium hexafluoroantimonate compound) to polymeric silica sols made by a two-step procedure (A2**), designed to minimize the siloxane condensation rate and foster facile silica-surfactant supra-molecular self-assembly during film deposition. First, TEOS ($Si(OC_2H_5)_4$),

ethanol, water and HCl (mole ratios 1:4:1:5 x 10^{-5}) were heated at 60 °C for 90 min. This sol was diluted with ethanol (1 sol : 2 C_2H_5OH) followed by addition of water and HCl. Finally, surfactant and the PAG were added such that the final reactant mole ratios were 1 TEOS : 20 C_2H_5OH : 3.1 H_2O : 0.0065 HCl : 0.0956 Brij 56 : 0.0156 PAG.

12. C. J. Brinker, G. W. Scherer, *Sol-Gel Science* (Academic Press, San Diego, 1990), pp. 139-142.

13. C. J. Brinker, et al., *Access in Nanoporous Materials*. T. J. Pinnavaia, M. F. Thorpe, Eds. (Plenum, New York, 1995), pp. 123-139.

14. Films were deposited on (100)-silicon by dip-coating at 25.4 cm/min. Following film deposition, the samples were irradiated with short-wave ultraviolet (UV) light for 2 hr through a mask via proximity printing to effectively transfer the pattern onto the silica thin film. Etching of the films was performed using a 0.2 M aqueous NaOH solution for a period of 5 to 10s. Calcination treatments to promote continued siloxane condensation and remove surfactant templates and residual organics associated with PAG were conducted in air at 450 °C for 3 hours using a ramp rate of 1°C/min. HCl exposures of unirradiated films were performed by placement in a chamber containing dispersed droplets of concentrated HCl for 2 hr.

15. C. J. Brinker, Y. F. Lu, A. Sellinger, H. Y. Fan, *Advanced Materials* **11**, 579-585 (1999).

16. J. V. Crivello, J. H. W. Lam, *Macromolecules* **10**, 1307-1315 (1977).

17. In aqueous solution ethyl violet is violet-blue for pH ≥ 2 and yellow for pH < 0

18. MAS ^{29}Si-NMR indicates an extent of condensation of 82.1% (Q2/Q3/Q4 =8.22/55.08/36.7) for irradiated, powdered films (2hr UV exposure) compared to 80.8% (Q2/Q3/Q4 =9.61/57.75/32.64) for the corresponding unirradiated samples. It can be expected that the condensation difference is much greater than the NMR value immediately after

irradiation, but lengthy acquisition times needed to perform the NMR experiment preclude our acquisition of data at '$t = 0$' and allow continued siloxane condensation to occur, diminishing this difference.

19. R. D. Miller, *Science* **286**, 421-423 (1999).

20. Using back-scattered electron emission imaging and energy dispersive X-ray spectrometry, we observed no evidence of compositional differences that could be responsible for the refractive index differences, so we conclude it is completely attributable to the optically defined phase transformation.

21. A. W. Snyder, J. D. Love, *Optical Waveguide Theory* (Chapman and Hall, New York, 1983), pp. 1-25.

22. J. T. Groves, N. Ulman, S. G. Boxer, *Science* **275**, 651-653 (1997).

23. We define the co-ordinate system to mainatin the *c* direction parallel to the cylinder axes of the as-deposited hexagonal mesophase. The two inplane directions (*b* and *c*) experience a constraint to shrinkage, whereas the *a* direction normal to the substrate is unconstrained and hence free to shrink, resulting in the smallest lattice constant. For the transformed mesophase the lattice constant *c* is determined from TEM (Fig 4B). Using *c* to solve the d_{111} spacing in the XRD pattern (Fig 3, trace B) we find *b*=*c*. In the case of the detached film fragments, the absence of any constraint from the substrate and the symmetry of the parent 1-dH mesophase cause the *a* and *b* lattice parameters to be the same in the transformed mesophase.

24. The (200) and (400) reflections of the tetragonal phase can also be indexed as the (100) and (200) reflections of the untransformed parent 1-dH mesophase.

25. R. K. Iler, *The Chemistry of Silica* (Wiley-Interscience, New York, 1979), pp. 213-215.

26. Any in-plane strain is resisted by attachment of the film to the substrate and results in the development of a bi-axial tensile stress in the plane parallel to the substrate surface as measured by a cantilever beam technique (32). We used this cantilever beam technique to monitor the polymerization-induced stress development during UV irradiation and subsequent heating for thin film mesophases prepared with and without the photo-acid generator. UV irradiation caused the development of 4 MPa of biaxial tensile stress for the irradiated film compared to approximately zero stress for the unirradiated film after 60 min of irradiation. (see auxiliary Figure A). Heating to 125°C, at which temperature the 1dH to tetragonal transformation occured, resulted in the development of an addditional 48 MPa of stress for the irradiated film compared to 18 MPa for the unirradiated film (see auxiliary Figure B).

27. J. Israelachvili, *Intermolecular and Surface Forces* (Academic Press, 1992), pp. 341-389.

28. J. N. Israelachvili, D. J. Mitchell, B. W. Ninham, *J. Chem. Soc.* **2**, 1525-1568 (1976).

29. A. Monnier, et al., *Science* **261**, 1299-1303 (1993).

30. P. Sakya, J. M. Seddon, R. H. Templer, R. J. Mirkin, G. J. T. Tiddy, *Langmuir* **13**, 3706-3714 (1997).

31. In an initial study of the effects of surfactant and acid concentration on mesophase development, we observed samples prepared with 3 wt% Brij-56 surfactant and without PAG to exhibit a 1-dH mesophase after deposition and after calcination. Samples prepared with 3wt% Brij-56, but with a higher acid concentration exhibited a 1-dH → tetragonal transformation upon heating. Similarly samples prepared with 4 wt% Brij-56 and without PAG exhibited a 1-dH → tetragonal transformation upon heating. Through introduction of PAG followed by UV irradiation and heating we are able to realize the 1-dH → tetragonal transformation for the 3 wt% Brij-56 specimen.

32. J. Samuel, C. J. Brinker, L. J. D. Frink, F. van Swol, *Langmuir* **14**, 2602-2605 (1998).

33. We thank C. Braunbarth for discussions about the phase transformation. We also thank R. Assink for assistance with NMR experiments and Y. Guo for assistance with TEM. This work was partially supported by the UNM/NSF Center for Micro-Engineered Materials, FWF Austria and the DOE Basic Energy Sciences Program. This work was done under contract from the US Department of Energy. Sandia is a multiprogram laboratory operated by Sandia Corporation, a Lockheed Martin Company, for the United States Department of Energy under contract DE-AC04-94AL85000.

Table 1 : Ellipsometry data showing thickness (t) and refractive index (n) (at λ = 630nm) for B56 films

	As-prepared Films		Calcined Films	
	t (Å)	n	t (Å)	n
Unirradiated	3651±26	1.454±0.001	2293±22	1.302±0.002
UV Irradiated	3602±21	1.457±0.001	2399±23	1.277±0.002

Figure. 1. Processing map for optically-mediated patterning of thin film silica mesophases.

Figure. 2. Optical patterning of function/properties in thin-film silica mesophases. (**A**) Optical image of localized acid generation via co-incorporation of a pH-sensitive dye (ethyl violet). The blue areas observed for the unexposed film correspond to pH* ≥ 2.0 and the yellow areas observed for the exposed film to pH* ~ 0 (where pH* refers to the equivalent aqueous solution pH required to achieve the same colors) (**B**) Optical micrograph of a UV-exposed and selectively etched mesostructured thin film (after calcination). Feature size ≈ 10 μm. Inset : TEM image of the film seen in (**B**) consistent with the [110]-orientation of a 1-dH mesophase with lattice constant a = 37 Å. (**C**) Optical interference image showing thickness and refractive index contrast in a patterned, calcined film. The green areas correspond to UV-exposed and calcined regions and the black areas to unexposed and calcined regions. (**D**) Optical image of an array of water droplets contained within patterned hydrophilic-hydrophobic corrals. Water droplets sit on hydrophilic regions with contact angle <10° and are bounded by the hydrophobic UV-exposed regions with contact angle = 40°.

Figure 3 X-ray diffraction patterns of calcined thin-film silica mesophases. Trace A: unirradiated film pattern, consistent with a 1-dH mesophase with lattice constant a = 42.1 Å . Trace B: irradiated film pattern, consistent with a tetragonal mesophase with a = 66.8 Å $b = c$ = 72.8 Å along with parent 1-dH mesophase with a = 38.5 Å. Trace C:

an unirradiated film exposed to HCl vapors and then calcined. The pattern is similar to the one obtained for the irradiated film (trace B) but with lattice constants a = 74.2 Å, b = c = 82 Å for the tetragonal mesophase and a = 43 Å for the 1-dH mesophase.

Figure 4 Cross-sectional TEM images of patterned film. (**A**) [110]-orientation of unirradiated calcined region prepared as in Fig 3 trace A. Striped pattern is consistent with 1-dH mesophase with a = 37 Å. (**B**) Irradiated calcined region prepared as in Fig 3 trace B capturing the 1-dH → tetragonal mesophase transformation. Inset: magnified image showing relationship between the 1-dH and tetragonal mesophases and defining the a and c lattice constants of the transformed tetragonal mesophase.

Figure 5 Powder X-ray diffraction pattern for calcined silica/surfactant mesophases. (**A**) pattern for the unirradiated powder is consistent with a 1-dH mesostructure with lattice constant a = 52.8 Å. High 2θ region is magnified by 25x (**B**) pattern for UV-irradiated powder is consistent with tetragonal mesophase with a = b = 81.5 Å, c = 107.8 Å. High 2θ region is magnified by 175x. Note that the (200) and (400) reflections of the tetragonal mesophase could also be indexed as (100) and (200) reflections of a 1dH mesophase with a = 47.4 Å

Figure 6 TEM images of calcined powder samples. (**A**) Unirradiated powder corresponding to the [110]-orientation of a 1-dH mesophase. (**B**) UV-irradiated powder corresponding to the [001]-orientation of a tetragonal mesophase.

Figure 7 Schematic diagram showing the mechanism of the transformation from the 1-dH mesophase (top) to a tetragonal (distorted cubic) mesophase (bottom). As condensation of the siloxane framework proceeds, the framework charge density decreases relative to that of the EO headgroups. The corresponding increase in the optimal surfactant headgroup area drives the 1-dH to tetragonal mesophase transformation through a periodically undulating intermediate as known for the thermally driven 1-dH $\rightarrow$ body-centered-cubic transformation of of $C_{12}EO_{12}$ in the $C_{12}EO_{12}/H_2O$ binary system (30).

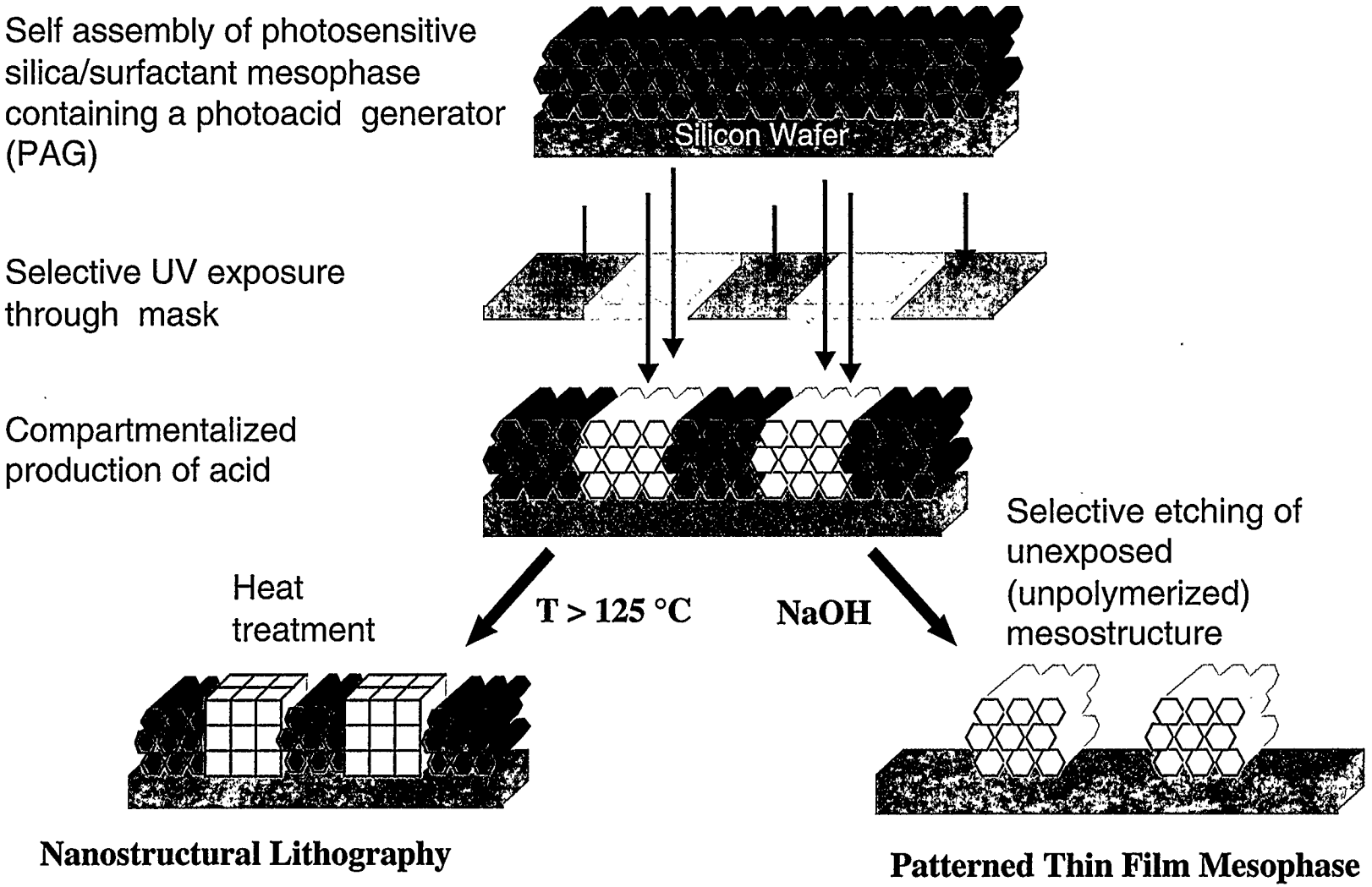

Figure. 1. Processing map for optically-mediated patterning of thin film silica mesophases.

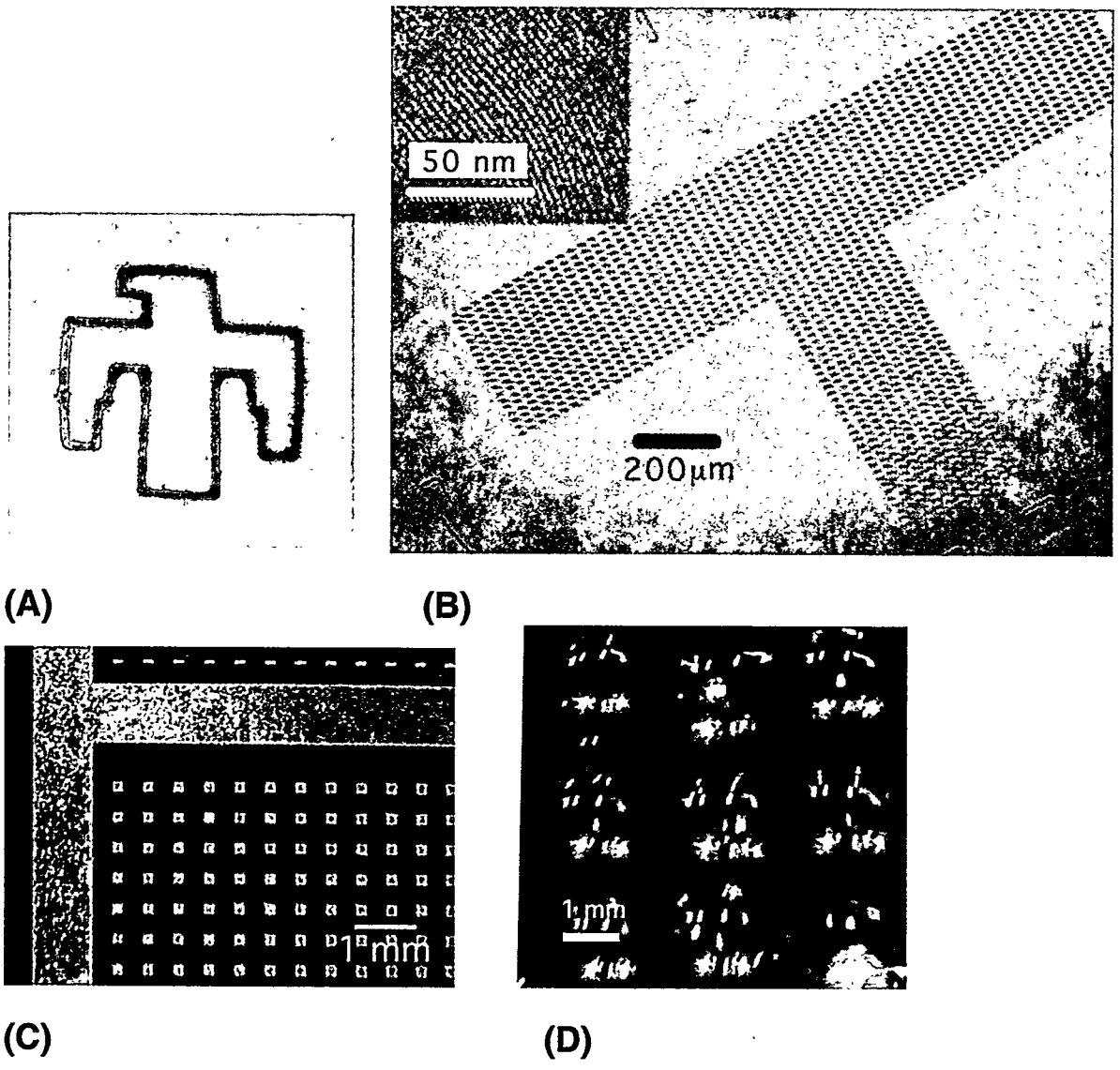

Figure. 2. Optical patterning of function/properties in thin-film silica mesophases. **(A)** Optical image of localized acid generation via co-incorporation of a pH-sensitive dye (ethyl violet). The blue areas observed for the unexposed film correspond to pH* ≥ 2.0 and the yellow areas observed for the exposed film to pH* ~ 0 (where pH* refers to the equivalent aqueous solution pH required to achieve the same colors) **(B)** Optical micrograph of a UV-exposed and selectively etched mesostructured thin film (after calcination). Feature size ≈ 10 μm. Inset : TEM image of the film seen in **(B)** consistent with the [110]-orientation of a 1-dH mesophase with lattice constant a = 37 Å. **(C)** Optical interference image showing thickness and refractive index contrast in a patterned, calcined film. The green areas correspond to UV-exposed and calcined regions and the black areas to unexposed and calcined regions. **(D)** Optical image of an array of water droplets contained within patterned hydrophilic-hydrophobic corrals. Water droplets sit on hydrophilic regions with contact angle <10° and are bounded by the hydrophobic UV-exposed regions with contact angle = 40°.

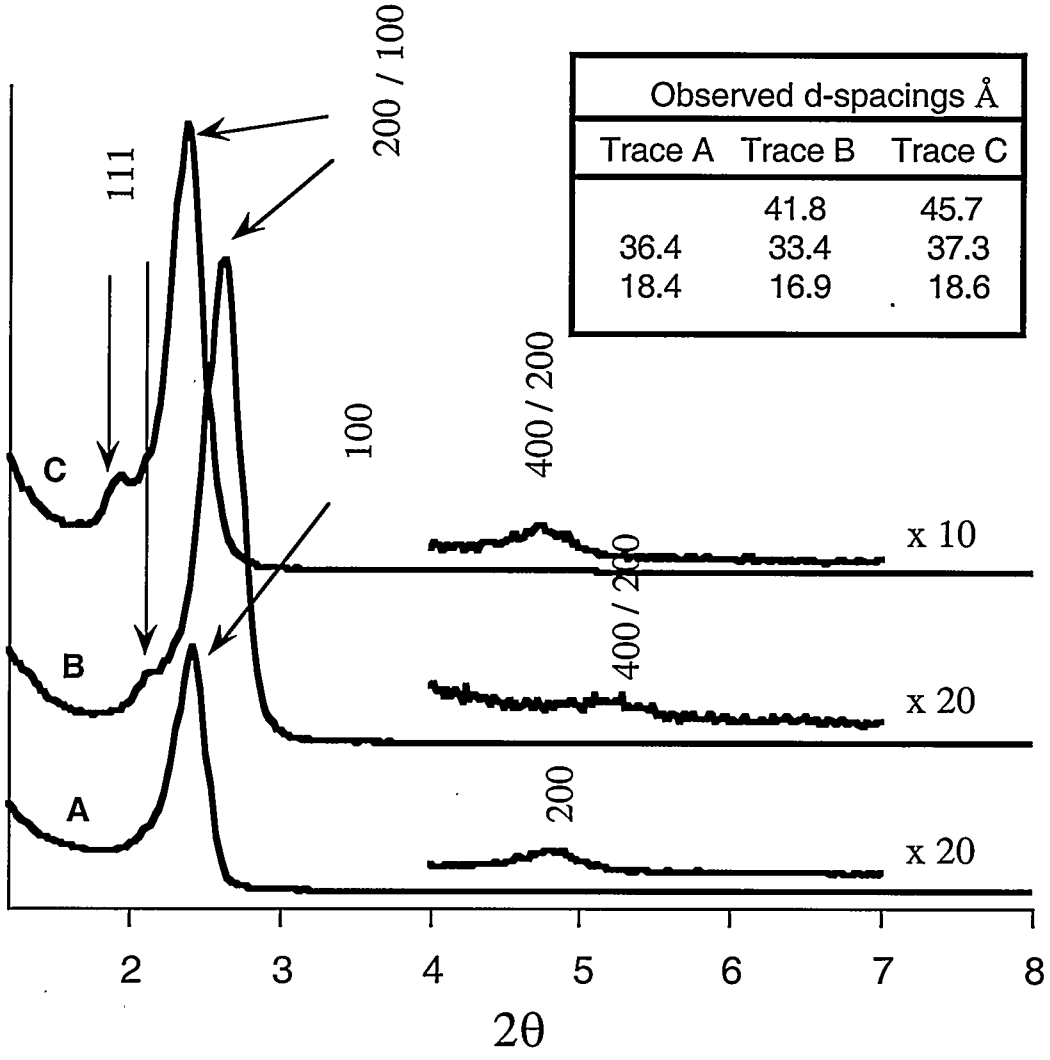

Figure 3 X-ray diffraction patterns of calcined thin-film silica mesophases. Trace A: unirradiated film pattern, consistent with a 1-dH mesophase with lattice constant a = 42.1 Å . Trace B: irradiated film pattern, consistent with a tetragonal mesophase with a = 66.8 Å b = c = 72.8 Å along with parent 1-dH mesophase with a = 38.5 Å. Trace C: an unirradiated film exposed to HCl vapors and then calcined. The pattern is similar to the one obtained for the irradiated film (trace B) but with lattice constants a = 74.2 Å, b = c = 82 Å for the tetragonal mesophase and a = 43 Å for the 1dH mesophase.

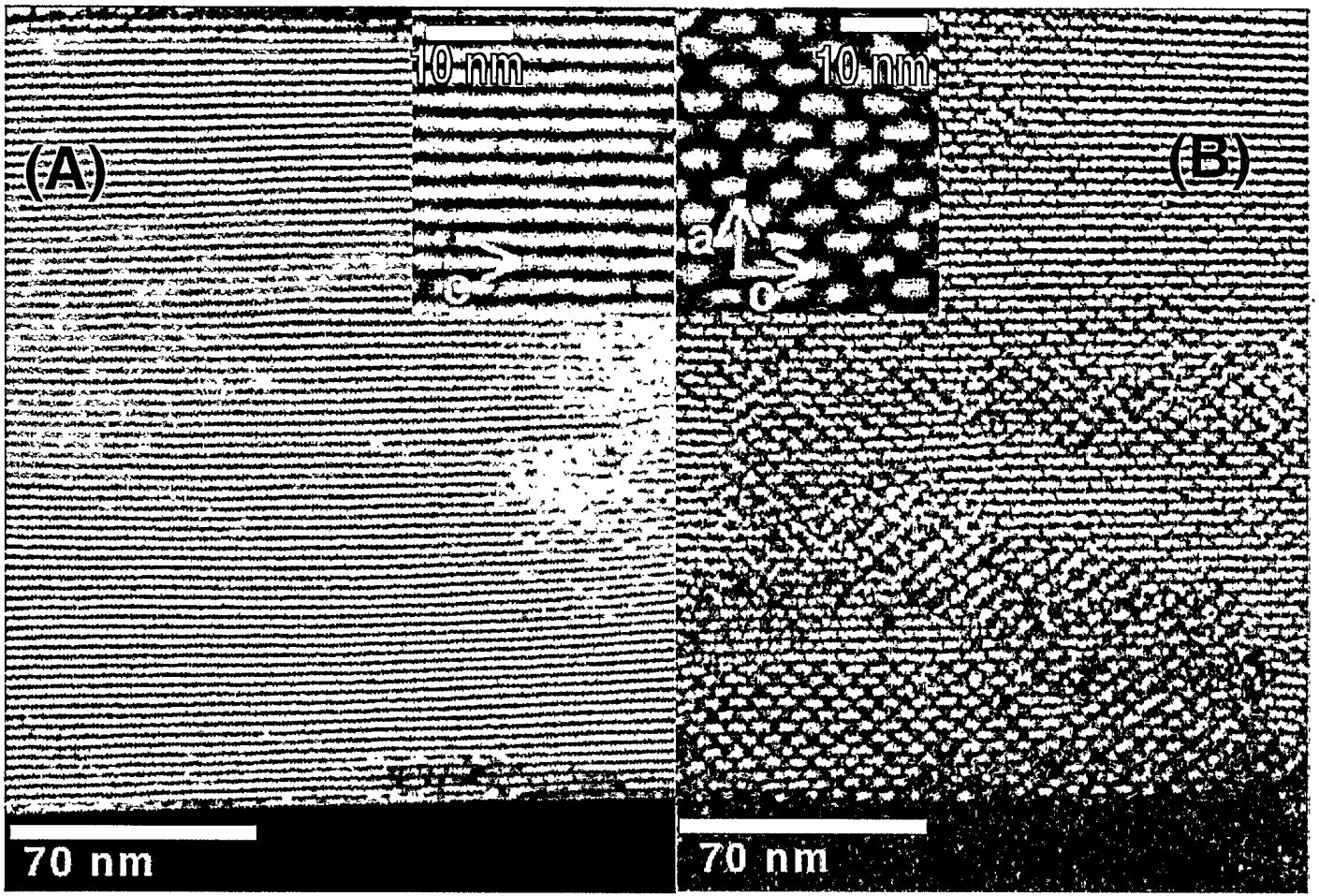

Figure 4 Cross-sectional TEM images of patterned film. (**A**) [110]-orientation of unirradiated calcined region prepared as in Fig 3 trace A. Striped pattern is consistent with 1-dH mesophase with a = 37 Å. (**B**) Irradiated calcined region prepared as in Fig 3 trace B capturing the 1-dH → tetragonal mesophase transformation. Inset: magnified image showing relationship between the 1-dH and tetragonal mesophases and defining the a and c lattice constants of the transformed tetragonal mesophase.

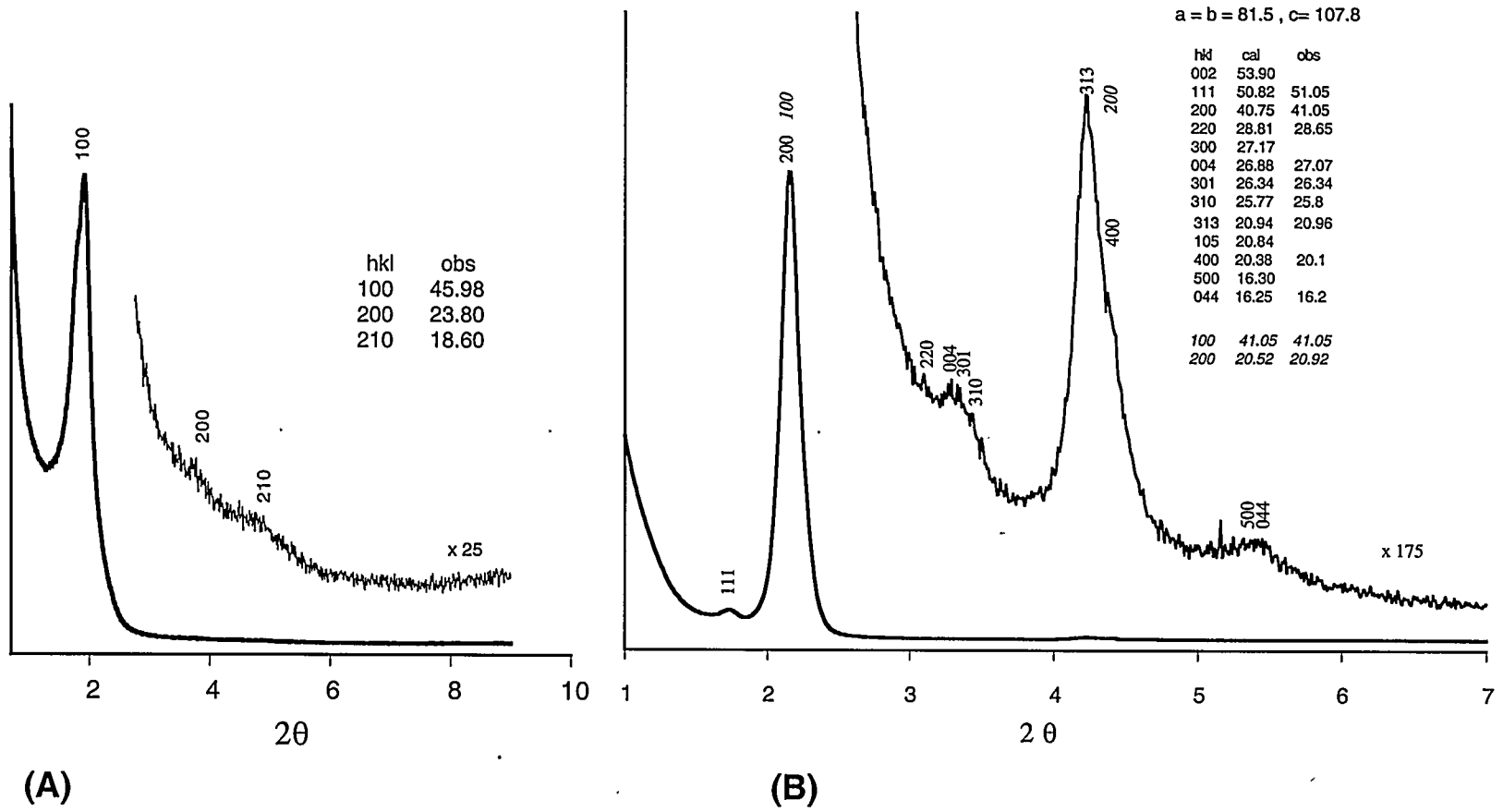

Figure 5 Powder X-ray diffraction pattern for calcined silica/surfactant mesophases. (**A**) pattern for the unirradiated powder is consistent with a 1-dH mesostructure with lattice constant a = 52.8 Å. High 2θ region is magnified by 25x (**B**) pattern for UV-irradiated powder is consistent with tetragonal mesophase with $a = b$ = 81.5 Å, c = 107.8 Å. High 2θ region is magnified by 175x. Note that the (200) and (400) reflections of the tetragonal mesophase could also be indexed as (100) and (200) reflections of a 1-dH mesophase with a = 47.4 Å

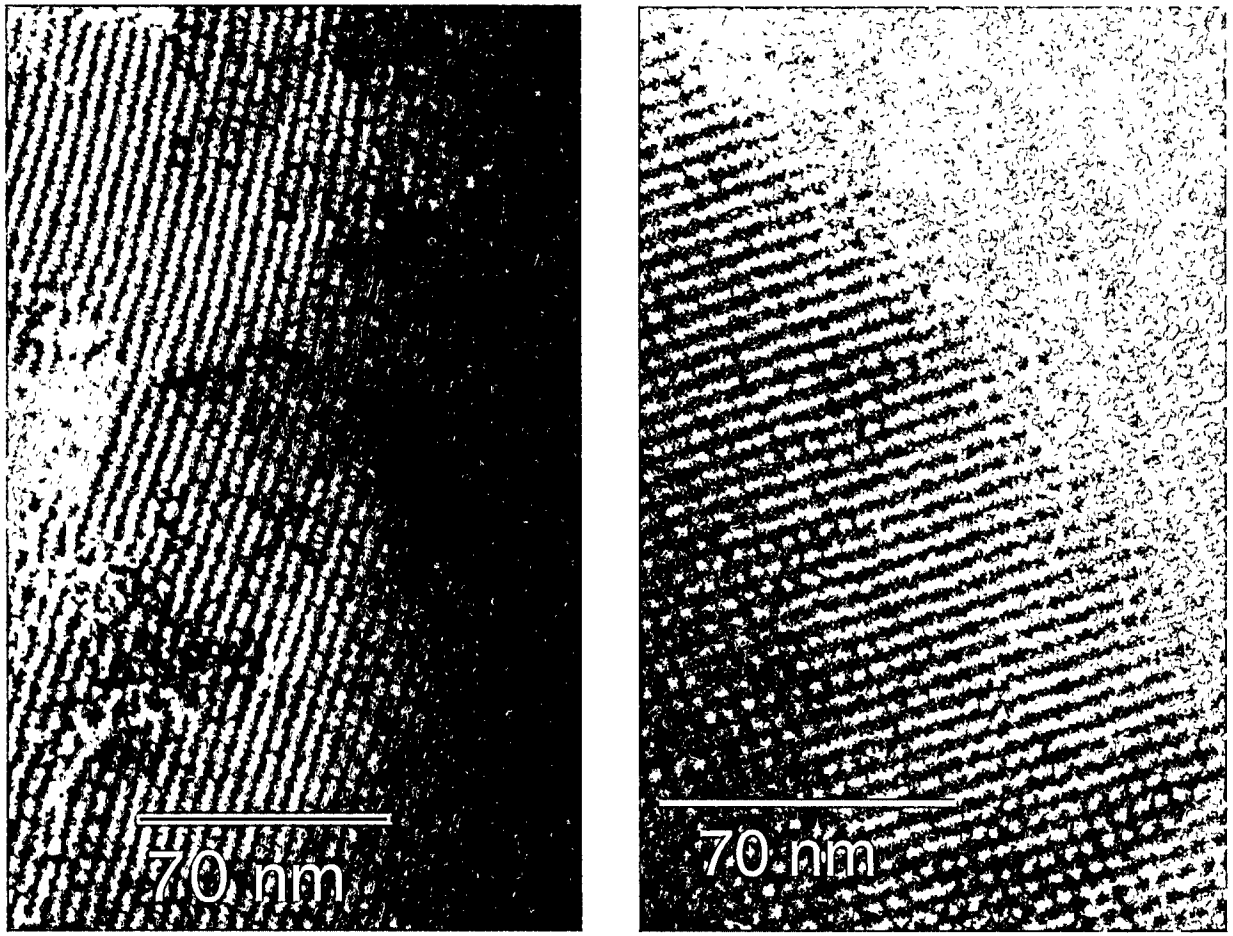

Figure 6 TEM images of calcined powder samples. (**A**) Unirradiated powder corresponding to the [110]-orientation of a 1-dH mesophase. (**B**) UV-irradiated powder corresponding to the [001]-orientation of a tetragonal mesophase.

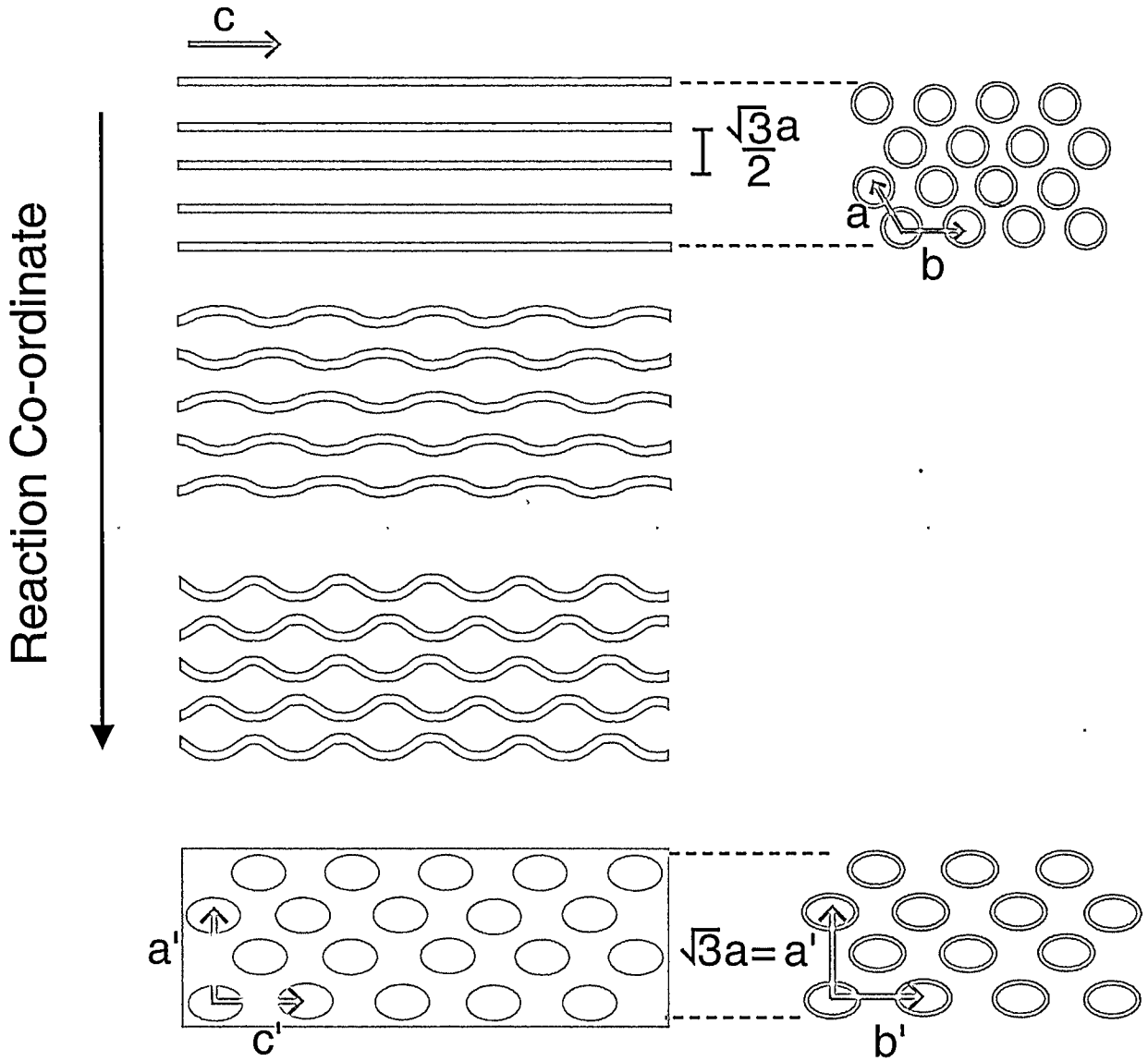

Figure 7 Schematic diagram showing the mechanism of the transformation from the 1-dH mesophase (top) to a tetragonal (distorted cubic) mesophase (bottom). As condensation of the siloxane framework proceeds, the framework charge density decreases relative to that of the EO headgroups. The corresponding increase in the optimal surfactant headgroup area drives the 1-dH to tetragonal mesophase transformation through a periodically undulating intermediate as known for the thermally driven 1-dH → body-centered-cubic transformation of of $C_{12}EO_{12}$ in the $C_{12}EO_{12}/H_2O$ binary system (30).

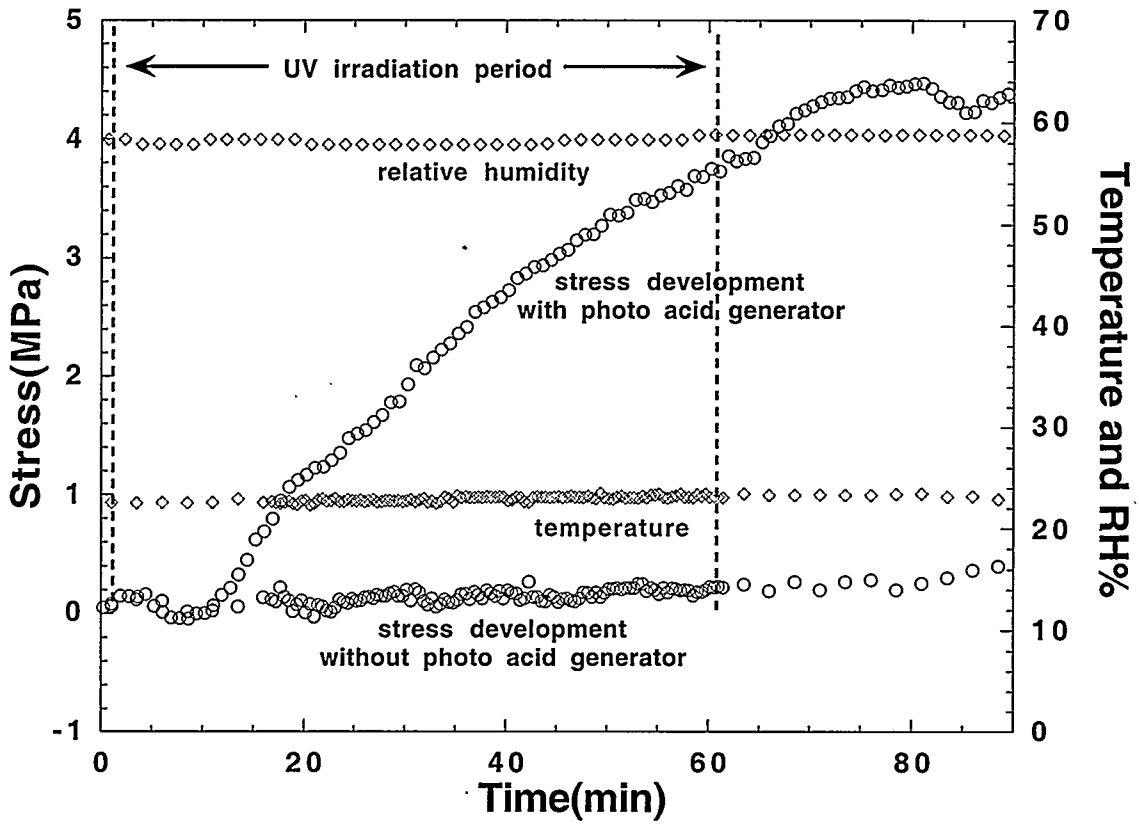

Auxiliary Figure A : Stress development during UV irradiation for films prepared with and without PAG. Development of 4.5 MPa of biaxial tensile stress is observed for films with PAG after UV irradiation of 60 min, whereas negligible stress develops for films prepared without PAG under similar conditions.

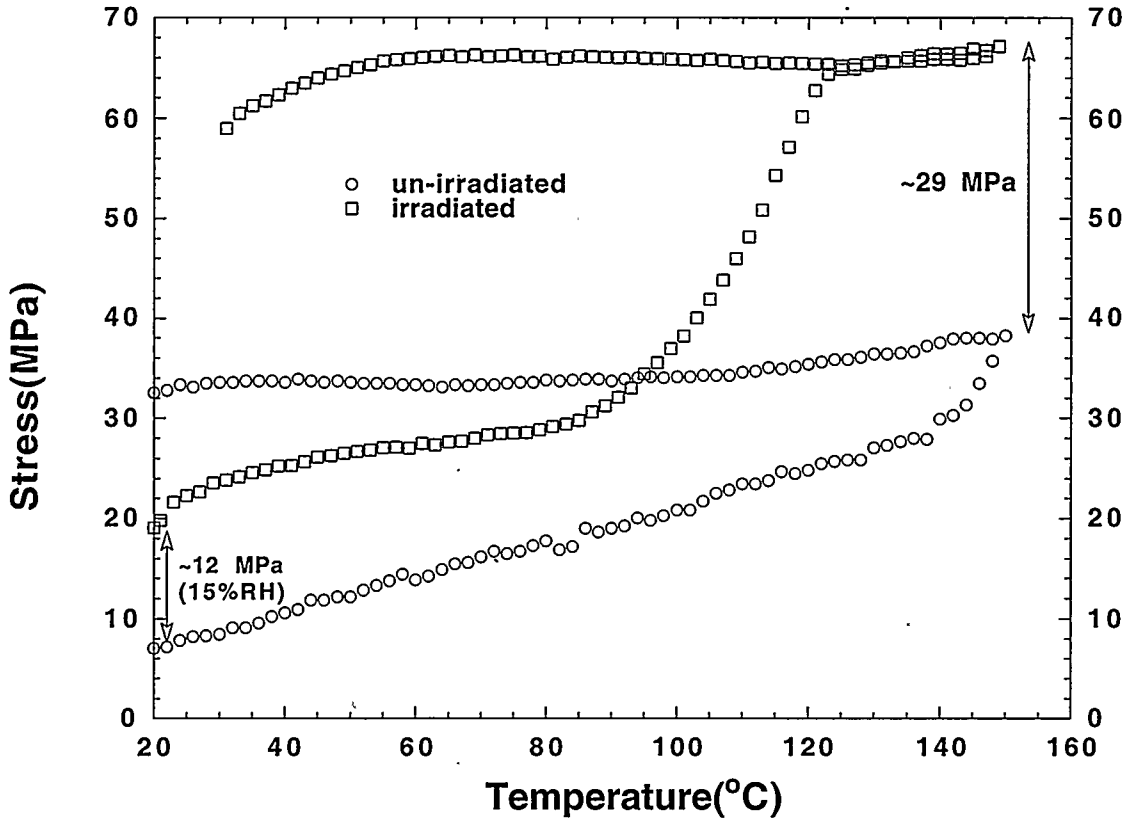

Auxiliary Figure B: Biaxial tensile stress development during the initial stage of calcination for irradiated and unirradiated films prepared with PAG. The irradiated film shows a higher initial stress at room temperature due to acid-promoted siloxane condensation. Upon heating to 150 °C, the irradiated film develops an additional 48MPa of stress whereas the unirradiated film develops an additional 30MPa.